Phonon Emission Induced Dynamic Fracture Phenomena

F. Atrash,[1] A. Hashibon,[2,3] P. Gumbsch,[2,3] and D. Sherman[1]

[1]*Department of Materials Engineering, Technion, Haifa-32000, Israel*

[2]*Fraunhofer-Institut für Werkstoffmechanik IWM, Freiburg-79108, Germany*

[3]*IZBS–Institut für Zuverlässigkeit von Bauteilen und Systemen, Karlsruher Institut für Technologie (KIT), 76131 Karlsruhe, Germany*

(Received 25 August 2010; revised manuscript received 23 December 2010; published 23 February 2011)

We use molecular dynamics simulations to calculate the phonon energy emitted during rapid crack propagation in brittle crystals. We show that this energy is different for different crack planes and propagation directions and that it is responsible for various phenomena at several length scales: energetically preferred crack systems and crack deflection at the atomic scale, reduced maximum crack speed with volume at the micrometer scale, and the inability of a crack to attain the theoretical limiting speed at the macroscale. We propose to include the contribution of this energy in the Freund equation of motion of a dynamically propagating crack.

DOI: 10.1103/PhysRevLett.106.085502 PACS numbers: 62.20.mj, 02.70.Ns, 46.50.+a, 63.20.dd

Crack speed and crack surface features originate from atomistic scale events and are determined by a discrete sequence of an enormous number of bond ruptures, each occurring on a time scale of less than a picosecond and must satisfy precise energy conservation laws. This is true for physical phenomena that span many orders of magnitudes of length scales, from crack propagation in Earth's crust to fracture in submicrometer scale devices.

The existing treatment of crack dynamics in brittle materials is based on continuum elasticity, and is determined by an energy balance through the Freund equation of motion [1]. The strain energy released when a crack advances by a unit area G_0 is consumed by the energy to create new surfaces $\Gamma(V)$ and by the energy dissipated by the elastic waves generated during propagation $G_K(V)$, where V is the crack speed. Freund formulated the net energy to break the bonds at the crack surface as the product of G_0 and a universal dynamical function $G_d(V)$. In a continuum mechanical treatment, he showed that $G_d(V)$ may be approximated as a linear function of the crack speed [1] for propagation at a constant speed V:

$$\Gamma(V) = G_0 G_d(V) \sim G_0\left(1 - \frac{V}{C_R}\right). \quad (1)$$

At low crack speed, propagation takes place when $\Gamma(V) = 2\gamma$, the Griffith energy [2], which is the lower bound for the energy required to generate new surfaces. It is important to note that the term $G_0(V/C_R)$ in Eq. (1) approximates G_K, the elastic wave energy release rate (ERR) only, designated by us as G_{El}. This term does not account for the atomistic nature of matter. The speed scale parameter C_R in Eq. (1) is the Rayleigh free surface wave speed, considered by Stroh [3] as the crack speed limit in solids. However, experiments [4–13] and atomistic computer simulations [14–16] have shown that the maximum speed a crack can attain is only 70%–90% of C_R. Moreover, fracture experiments of silicon specimens under bending [11,13] have shown crack deflection from (110) to (111) cleavage plane of silicon. These two phenomena indicate that additional energy dissipation mechanisms should exist.

We study by atomistic simulations the contribution of the thermal phonon energy to the ERR in dynamic fracture. While this energy was previously suggested as a possible energy dissipation mechanism [11–13,16–18], thorough analysis has not yet been performed. Here we show that the phonon ERR is the missing link in the equation of motion; it allows us to interpret critical aspects in dynamic fracture such as limiting crack speed and surface instabilities. In addition, we point out the multiscale effect of this energy dissipation mechanism.

We investigated energy dissipation during dynamic crack propagation for a variety of crack speeds in diamond-cubic silicon, which has two preferred low energy cleavage planes, (111) and (110). We used molecular dynamics (MD) simulations to evaluate the contribution of the phonon emission to the dynamical ERR in a model system silicon crystal. In this study, we use the modified Stillinger-Weber (SW) potential [15] to describe a model of a brittle crystal with a diamond structure unit cell with lattice parameter 5.431 Å.

To study crack propagation, we used a precracked strip-like specimen, subjected to prescribed displacement on the boundaries, commonly used in atomistic simulations [14–16,18]. Samples consisting of about 120 000 atoms arranged in a diamond lattice were set up for the computational experiments. The dimensions of the specimens were about $450 \times 160 \times 20$ (in Å). Six different cleavage systems for a wide range of crack velocities were investigated. A precrack, 20% of the length of the specimen (nearly 40 atoms), was created by removing one atomic layer at the mid of the sample's height. The MD integration time step was set to 0.383 fs, which is 3 orders of magnitude smaller than the time unit equivalent to the Einstein

frequency of this potential [19]; i.e., both optical and acoustical phonons are simulated, which cannot be achieved by other discrete lattice models. In order to obtain the displacement field of a stable crack at zero temperature, the load was applied by quasistatic increments of homogeneous strain of 10^{-5} followed by a relaxation using a conjugate gradient method. These were applied up to fracture (total strain of $\sim 6 \times 10^{-2}$). The atomic configurations, just a few strain increments before fracture, were used as an input to microcanonical MD simulations. The initial velocities were set to distribute normally around a value that is equivalent to 10 K.

Periodic boundary conditions were employed along the sample's thickness direction z. The positions of the uppermost and lowermost two atomic layers were kept fixed during the relaxation and the MD simulation. The positions of the outermost left and right two atomic layers are free during relaxation but kept fixed during the MD simulations. To determine the energy dissipated by phonon emission over a relatively wide range of crack speeds, we stopped the MD simulations after the crack has ruptured about 20 bonds. We then rescaled homogeneously the entire strain field gradually in strain steps of $\sim 10^{-3}$ each to the desired level, which resulted in an increased or decreased crack tip speed. After this step the outermost two atomic positions layers of the model were kept fixed and the time evolution of the sample was again simulated with microcanonical MD. The stepwise loading changes the strain field homogeneously and thus can be used at any stage of the simulation and also prevents shock waves in the specimen [18]. Both the kinetic energy and crack tip position were calculated during crack propagation, their averages were calculated for the first 4 ps of the MD runs to avoid interaction between reflected waves and the crack tip. The IMD [20] code was used to conduct the conjugate gradient relaxations and MD simulations. The strain ERR in our systems is given by

$$G_0 = \tfrac{1}{2} H E^* \bar{\varepsilon}^2, \tag{2}$$

where $\bar{\varepsilon}$ is the final remote applied strain normal to the crack surface direction and H is the height of the specimen. The effective secular elastic constant E^* in Eq. (2) is determined in separate calculations using the modified SW interatomic potential; E^* vary nearly linearly with $\bar{\varepsilon}$, where $dE^*/d\bar{\varepsilon}$ is approximately 8 GPa for each 1% strain for all the cleavage systems. For a crack propagating at a constant velocity V, the total kinetic ERR G_k can be explicitly calculated by our MD simulations using

$$G_K^{\mathrm{MD}} = 2\frac{\partial E_K}{\partial A} = \frac{2}{bV}\frac{\partial E_K}{\partial t}, \tag{3}$$

where b is the width of the model and A is the crack surface area. The factor of 2 originates from the equipartition theorem; i.e., the waves emitted from the crack tip carry equal amounts of potential energy and kinetic energy E_K. A least squares routine was utilized to calculate the gradient of the kinetic energy. Similar methodology was used by Jin *et al.* [21] for dislocations dynamics.

It is important to note that the high frequency atomistic vibrations, or thermal phonons, cause thermal expansion and partial relaxation of the strain tensor near the crack tip. It is hence reasonable to assume that G_0 in Eq. (1) available to drive the crack reduces by G_{ph}, and the reduced speed V is that obtained in the MD calculations. G_K^{MD} contains both the contributions of the elastic waves and the phonon ERR, namely, $G_K^{\mathrm{MD}} = G_{\mathrm{El}} + G_{\mathrm{ph}}$. G_{El} was calculated from Eq. (1) using the reduced speed V and G_{ph} by subtracting G_{El} from G_K^{MD}:

$$\frac{G_{\mathrm{ph}}}{2\gamma} \approx \frac{G_K^{\mathrm{MD}}}{2\gamma} - \frac{V}{C_R}\left(1 - \frac{V}{C_R}\right)^{-1}. \tag{4}$$

The elastic constants vary along the crack propagation direction, and therefore C_R is not a direct function of the strains. Hence, we chose to use C_R of the relaxed crystal. The anisotropic C_R [22] was calculated by the modified SW potential (see values in [23]) for each cleavage system. We analyzed six crack systems, shown in the inset of Fig. 1(a). Several phenomena are evident from these calculations: G_{ph} at $V < 0.4C_R$ is small, becomes significant at $V > 0.5C_R$, and prevents the crack from attaining C_R. In addition, G_{ph} is influenced by crystal anisotropy, as the terminal speed bounds between $0.52C_R$ and $0.64C_R$. Towards terminal speed cracks obviously attempt to run as fast as possible and will choose the crack system that permits the highest speeds. This can even lead to changes in preferred crack systems: at $V > 0.4C_R$, cracks on the

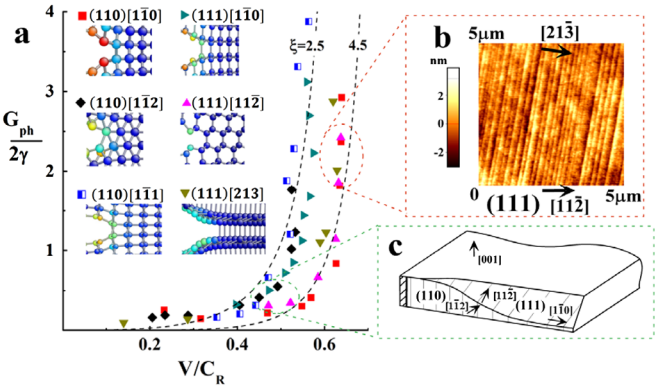

FIG. 1 (color online). (a) The normalized phonon emission ERR, $G_{\mathrm{ph}}/2\gamma$, as a function of the normalized crack speed, V/C_R, for six cleavage systems (first brackets denote the cleavage plane, the second the crack propagation direction) obtained by Eq. (4). The energy dissipated by phonon emission increases rapidly around $V/C_R > 0.5$, which may describe surface phenomena such as in-plane anisotropy of the silicon (111) cleavage plane as shown in the (b) AFM image of the fracture surface of cleaved silicon specimen under tension, at speed larger than $0.5C_R$. The subnanoscale ridges indicate that the crack is propagating in the $[21\bar{3}]$ direction. The anisotropic phonon ERR also explains the deflection phenomenon in silicon under bending [11,13] schematically shown in (c) crack deflected primarily from$(110)[1\bar{1}2]$ to $(111)[11\bar{2}]$ at $V > 0.45C_R$. The dashed lines in (a) were calculated by Eq. (6).

(111) cleavage plane prefer to propagate in the $[11\bar{2}]$ and $[21\bar{3}]$ directions over the $[1\bar{1}0]$ direction. We observed this phenomenon on the fracture surface of silicon, cleaved on the $(111)[11\bar{2}]$ cleavage system under tension (see [7] for details of experiments). The fracture surface depicted by an atomic force microscope (AFM) scan (where $V > 0.5C_R$), demonstrated inclined ridge patterns at an angle that coincides with the $[21\bar{3}]$ direction, as shown in Fig. 1(b). While $G_{\rm ph}$ [Fig. 1(a)] was similar for the $[11\bar{2}]$ and $[21\bar{3}]$ directions, the experiment showed that the latter is preferred. Furthermore, cracks on the (110) cleavage plane prefer the $[1\bar{1}0]$ direction over the $[11\bar{1}]$ and the $[1\bar{1}2]$ directions [Fig. 1(a)]. This is again in excellent agreement with previous experimental results [8] which showed that the $[1\bar{1}0]$ direction is preferred on the (110) cleavage plane in single crystal silicon.

The macroscopic crack deflection observed in bending cleavage experiments of silicon [11,13] can be rationalized with the anisotropy of $G_{\rm ph}$, Fig. 1(a). Our calculations predict that cracks propagating on the $(110)[1\bar{1}2]$ system will deflect to the least energetic $(111)[11\bar{2}]$ system at $V/C_R \sim 0.45$. This is in good agreement with experiments [11,13], as schematically shown in Fig. 1(c). The calculations also predict that crack propagation on the $(110)[1\bar{1}0]$ system will not deflect to the $(111)[1\bar{1}0]$ system, as $G_{\rm ph}$ in the former is smaller. This is also shown in experiments presented in [11,13] and schematically shown in Fig. 1(c).

Next, we suggest incorporating $G_{\rm ph}$ in the Freund equation [Eq. (1)]. We first modeled $G_{\rm ph}$ as if it is generated by a line heat source, attached to the moving crack front at constant speed V, in an infinite isotropic body, whose temperature profile is [24]

$$\Delta T(r, \theta, V) = Q(V/2\pi\kappa)\exp[-Vr\cos\theta/2\lambda]K_0(Vr/2\lambda),$$

where κ and λ are the thermal conductivity and diffusivity, respectively, K_0 is the second kind zero order Bessel function, Q the thermal energy, and r and θ are the coordinates from the crack tip. $G_{\rm ph}$ was calculated by the Rice J integral, in the same way the elastic waves were treated by Freund [1]:

$$G_{\rm ph} = 2\int_{\bar{\Gamma}} \frac{3}{2} k_B \Delta T(r, \theta, V)\rho n_1 d\bar{\Gamma} = Q\frac{V}{A}\exp\left(-\frac{V}{B}\right)K_0\left(\frac{V}{B}\right), \quad (5)$$

where n_1 is a unit vector directed normal to the path Γ, which coincides with the sample boundaries, $A = 2\pi\kappa/(3\rho k_B H)$, $B = 2\lambda/L$, ρ the atomic density, and L and H the width and height of the specimen, respectively. $G_{\rm ph}$ in the form of the right-hand side of Eq. (5) was added to the right-hand side of Eq. (1). The resultant V/C_R vs $G_0/2\gamma$ (see parameters in [25]) is shown by the dash-dotted red line in Fig. 2 together with the Freund equation. Obviously, $G_{\rm ph}$ from Eq. (5) brings in terms of higher order in V/C_R that reduces the speed of the crack.

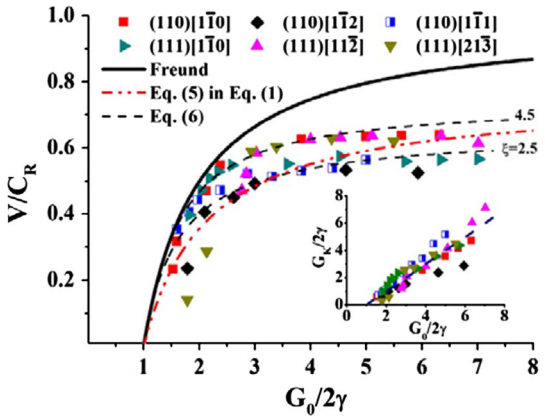

FIG. 2 (color online). V/C_R vs $G_0/2\gamma$ for the six cleavage systems obtained by our MD calculations. The solid line is the Freund equation of motion [1] [Eq. (1)]. The extended Freund equation of motion containing the phonon ERR by the line heat source model, Eq. (5), is shown by the red dot-dashed line and by our MD calculations, Eq. (6), by dashed lines, with two limiting values of the material parameter, $\xi = 2.5$ and 4.5. The inset shows that $G_0 = G_K + 2\gamma$, and, presumably, no other energy dissipation mechanisms exist.

Normalized crack speed as a function of normalized driving force as obtained by our MD simulations is also shown for all six cleavage systems in Fig. 2. Differences in the different simulation results are attributed to the crystal anisotropy, the finite volume of the simulated model, and the temperature dependency of the material parameters. Based on the above, one possible way to incorporate a crack system specific $G_{\rm ph}$ in the Freund equation of motion [1] is by using a power law of V/C_R [justified by Eq. (5)], and hence we rewrite Eq. (1) in the following form:

$$\Gamma(V) = G_0\left[1 - \frac{V}{C_R} - \left(\frac{V}{C_R}\right)^{\xi}\right]. \quad (6)$$

The power ξ then is a phenomenological material parameter which depends among other factors on the anisotropy of the crystal and the volume of the cracked body. Our MD calculations were best fitted when $\xi \sim 2.5$–4.5, as shown in Figs. 1(a) and 2. Note the good agreement between $G_{\rm ph}$ obtained by our MD calculations with $G_{\rm ph}$ of Eq. (5) substituted into Eq. (1), as shown in Fig. 2. Higher values of ξ imply that the phonon energy dissipated is lower. The limiting velocity that a crack can attain, $V_{\rm max}$, for a given cleavage system is achieved at $G_0 \gg 2\gamma$, and thus Eq. (6) provides one-to-one relation between $V_{\rm max}$ and ξ. The reported experimental terminal velocities range between $0.7C_R$ and $0.9C_R$ [4,8,13]. According to Eq. (6), such velocities are possible with ξ values ranging between 6 and 30, meaning that phonon emission dissipates 21% to 6% of the strain energy inserted into the specimen, respectively. The relative amount of consumed energy may of course depend on system size and, hence, possible size effect must be considered.

We, therefore, calculated the terminal crack speed for different volumes of cracked bodies. Samples with the same

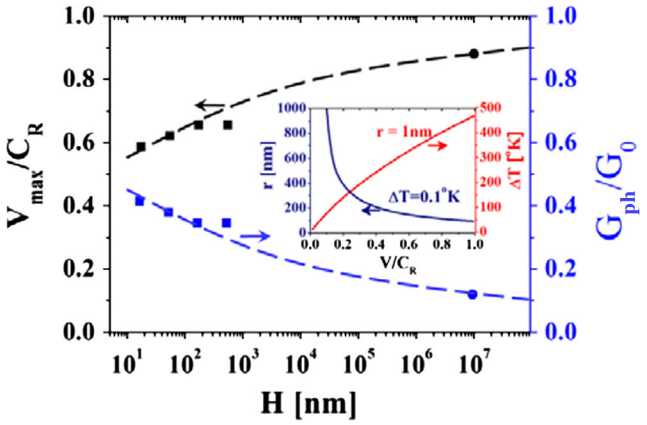

FIG. 3 (color online). The maximum normalized crack speed, $V_{\max}/C_R$, and the normalized phonon ERR, G_{ph}/G_0, as a function of the specimen height H obtained by our MD calculations (full squares) for the $(110)[1\bar{1}0]$ cleavage system and by experiments (full circle) [13]. The dashed lines show the trend. The radius of the hot zone and the maximum temperature as a function of crack speed, obtained by the temperature profile equation and the material parameters given in [25], are shown in the inset.

geometry and boundary conditions that contained 25 K, 250 K, 2.5 M, and 25 M atoms were analyzed, which corresponds to height, $H = 18, 55, 175, 553$ nm. The normalized terminal crack speeds, $V_{\max}/C_R$, vs the specimen height are shown in Fig. 3. It is evident that, as the volume of the cracked body decreases, the maximum crack speed decreases. For the 18 nm height specimen, the maximum crack speed was $0.58C_R$. The MD with semiempirical interatomic potential failed to evaluate crack speed above $0.65C_R$ in the largest volume, and nonlinear deformations prevailed.

Using the heat source model, we calculated the radius of the heated process zone, $r_{\mathrm{pz}} = r$ when $\Delta T \sim 0.1$ K (1% of the temperature of the unloaded atomistic model). For $V = 0.7C_R$, $r_{\mathrm{pz}} \sim 150$ nm. We therefore suggest that for height smaller than ~ 1 μm ($6r_{\mathrm{pz}}$), the heated zone is comparable with the height H; hence, the portion of the dissipated phonon ERR increases. At increased volume, the ERR dissipated by phonons is relatively small compared with the strain ERR in the body. More energy is then available for the bond breaking mechanisms, and crack speed increases; see Fig. 3. The volume effect is incorporated in Eq. (6) by the power ξ.

It is worth noting that we performed MD simulations of dynamic fracture at a temperature range of 10–300 K. The results showed that the terminal crack speed ($V_{\max}$) is not affected by the increased temperature (cf. [26]), meaning that G_{ph} is not affected by temperature at that range.

In summary, we showed that on the atomic scale, G_{ph} dictates the preferred direction of crack propagation and crack deflection. These results are in excellent agreement with experimental results. On the submicrometer scale, G_{ph} dictates the maximum crack speed, such that the maximum crack speed only reaches about $0.6C_R$, which is practical in fracture of nanotubes or graphene sheets. On the other hand, at the macroscale, this energy prevents the crack speed from attaining C_R, the theoretical limit speed, though this effect is relatively small in large volumes. It was shown that G_{ph} strongly depends on crack speed, volume, and on the atomistic arrangement at the crack tip. An additional term was suggested to the Freund equation of motion of a dynamically propagating crack. Consequently, the modified Freund equation of motion now can be utilized in a continuum-based model, such as finite element analysis.

A. Gleizer is acknowledged for the AFM analyses. F. A. acknowledges financial support by the Israeli Ministry of Science and Technology. P. G. acknowledges financial support by the German Research Foundation under Contract No. Gu 367/30. A. H. and F. A. acknowledge the support of the COST-STSM-P19-3693 mission. D. S. acknowledges funding from the EU-FP7-NMP Grant "ADGLASS."

[1] L. Freund, *Dynamic Fracture Mechanics* (Cambridge University Press, Cambridge, England, 1998).
[2] A. Griffith, Phil. Trans. R. Soc. A **221**, 163 (1921).
[3] A. Stroh, Adv. Phys. **6**, 418 (1957).
[4] T. Cramer, A. Wanner, and P. Gumbsch, Phys. Rev. Lett. **85**, 788 (2000).
[5] J. Fineberg *et al.*, Phys. Rev. Lett. **67**, 457 (1991).
[6] J. Hauch *et al.*, Phys. Rev. Lett. **82**, 3823 (1999).
[7] J. Kermode *et al.*, Nature (London) **455**, 1224 (2008).
[8] G. Michot, Surf. Sci. **186**, L561 (1987).
[9] J. Riedle, P. Gumbsch, and H. F. Fischmeister, Phys. Rev. Lett. **76**, 3594 (1996).
[10] K. Sauthoff *et al.*, Phys. Rev. B **60**, 4789 (1999).
[11] D. Sherman and I. Be'ery, J. Mech. Phys. Solids **52**, 1743 (2004).
[12] D. Sherman, M. Markovitz, and O. Barkai, J. Mech. Phys. Solids **56**, 376 (2008).
[13] D. Sherman, J. Mech. Phys. Solids **53**, 2742 (2005).
[14] N. Bernstein and D. W. Hess, Phys. Rev. Lett. **91**, 25501 (2003).
[15] D. Holland and M. Marder, Phys. Rev. Lett. **80**, 746 (1998).
[16] J. G. Swadener, M. I. Baskes, and M. Nastasi, Phys. Rev. Lett. **89**, 85 503 (2002).
[17] F. Abraham *et al.*, Phys. Rev. Lett. **73**, 272 (1994).
[18] P. Gumbsch, S. J. Zhou, and B. L. Holian, Phys. Rev. B **55**, 3445 (1997).
[19] F. H. Stillinger and T. A. Weber, Phys. Rev. B **31**, 5262 (1985).
[20] J. Stadler, R. Mikulla, and H. Trebin, Int. J. Mod. Phys. C **8**, 1131 (1997).
[21] Z. Jin, H. Gao, and P. Gumbsch, Phys. Rev. B **77**, 094303 (2008).
[22] A. Darinskii, Wave Motion **25**, 35 (1997).
[23] $C_R(111) = 5.94$, $C_R(110)[1\bar{1}0] = 5.55$, $C_R(110)[1\bar{1}1] = 5.94$, and $C_R(110)[1\bar{1}2] = 6.2$ all in (km/sec).
[24] H. Carslaw and J. Jaeger, *Conduction of Heat in Solids* (Oxford University Press, Oxford, 1959).
[25] Using $\kappa = 1.3$ W/cm °C, $\lambda = 0.8$ cm^2/s, $\rho = 49.94$ atom/nm^3, $H = 18$ nm, $L = 53$ nm, and $Q = G_0$.
[26] D. Holland and M. Marder, Adv. Mater. **11** 793 (1999).